MATHEMATICAL TREATMENT OF SUPERCONDUCTING LINEAR SYNCHRONOUS MOTOR

Tetsuzo Sakamoto
Department of Control Engineering, Kyushu Institute of Technology
Tobata, Kitakyushu 804, Japan

SUMMARY

The paper deals with the superconducting linear synchronous motor with application to the propulsion system of a high-speed transportation maglev vehicle. The system is composed of superconducting magnets (SCMs) on the vehicle and linear synchronous motor armature windings on the ground. The suitable coordinate system on the speed control may be *dq*-axis fixed on the SCMs.

The system variables are formulated viewing from the *dq0*-axes and the block diagram is constructed accordingly. A speed control system is then designed with appropriate disturbance compensations included, and it is confirmed from computer simulations that it works well under disturbed conditions.

INTRODUCTION

The superconducting linear synchronous motor (LSMs) is suitable for the propulsion of a high-speed transportation maglev vehicle; the power factor and efficiency are kept high even for a large gap between the superconducting magnets (SCMs) and the LSM armature windings.

There are mainly two types of operation for a synchronous motor in terms of the source voltage determination: they are "separately-controlled type" and "self-controlled type". On the former, the armature current flows in the circuit passively depending on the magnitude of the load. The current phase lags or leads from the source voltage, which is determined from the magnitude relation for the applied voltage and the speed emf induced from the field. The load is often referred to using the variable called load angle, because the phase angle between the applied voltage and the speed emf increases monotonically as the load increases, where no load corresponds to zero load angle. If the load exceeds the maximum value, which is called pullout power, then the motor loses synchronism. On the other hand, the source voltage of the self-controlled type is generated in such a way that the armature current flows in phase with the induced speed emf, which realizes zero lateral force, and high power factor. The current always lags behind the source voltage. In this case, however, the phase angle between the applied voltage and the induced speed emf never becomes zero for even no load. Accordingly the load angle does not mean the load magnitude for this type, and then it does not have a practical meaning. The applied voltage is produced by a variable voltage variable frequency (VVVF) power source according to the signals from position detectors. Therefore, this operation never loses synchronism as long as the detector works normally. This paper discusses the treatment of the self-controlled type linear synchronous motor.

Dawson et al. (ref. 1) discussed the fundamental characteristics of a superconducting LSM in a three-phase coordinate system assuming a fundamental component of magnetic field, and constructed a control system having vehicle speed and force angle as feedback signals, and voltage and frequency as

manipulated variables. Maki et al. (ref. 2) showed detailed computer simulations of electrodynamic variables in terms of three-phase coordinate system, but they did not refer to the combination with the control system. Although Ikeda presented a block diagram of the speed control system constructed in dq-axes (ref. 3), it ended up with a qualitative discussion with respect to electrodynamic variables. The author has presented an exact analysis of the propulsion system in $dq0$-axes with space harmonics of magnetic field included, and defined the thrust coefficient (ref. 4), making it possible to understand the characteristics quantitatively in a similar way as DC motor. The block diagram can be constructed almost exactly as it is in the practical maglev vehicle by using mathematical modeling, where any uncertainty is not retained in the formulation with respect to the propulsion system. Consequently, the three-power converter system employed at the new test track of Japan Railway in Yamanashi, where the propulsion power is supplied in sections from three inverters, is easily included in the block diagram. In this paper, the analysis is shown using the configurations of the test vehicles developed by Japan Railway.

ANALYSIS, MODELS, AND SPEED CONTROL SYSTEM

Propulsion force is provided by the interaction between the vehicle-borne SCMs and the armature windings with air core on the guideway. The SCMs are arranged in a concentrated manner so that the passenger cabin is not exposed into strong magnetic field, and at the same time the total weight of SCM becomes minimum.

Figure 1 shows the first of two models we discuss here, which has three SCM's arranged with two pole-pitch spaces in the longitudinal direction. The armature coil is installed in the form of two layers of 240-degree coil pitch arrangement as shown in the figure. The other form of armature coil has a single layer of 120-degree coil pitch, and it is treated as a special case for the 240-degree configuration in the formulation. The coordinate systems (x,y,z) and (x',y',z') are fixed on the vehicle and the guideway, respectively. The electromagnetic field problem is formulated through two stages: i) to derive the magnetic field equations considering the SCM as the source; ii) to formulate the interaction between the armature currents and the SCM's, i.e., induced emf, and forces. The magnetic field is derived by means of a magnetic vector potential or a magnetic scalar potential; the latter is simple. The physical meaning of using the magnetic scalar potential is to regard the SCM as a magnetic charge layer. Let the *mmf* function of SCM array located at $y = d_s$ be $f_s(x,z)$, and then the next equation holds

$$M_S = e_y f_S(x,z)/h_S \tag{1}$$

where M_s is the magnetization vector, e_y is the y-component unit vector, and h_s is the thickness of

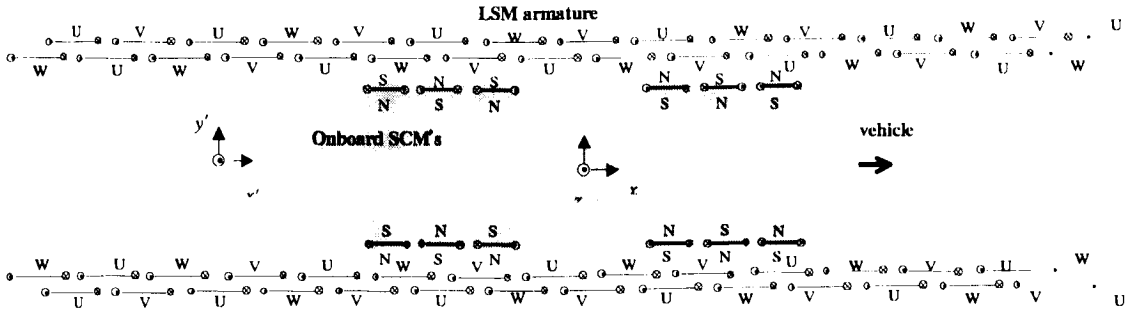

Figure 1. LSM armature windings and onboard SCM's (Model 1)

the SCM. Hence the magnetisation charge density is given by the divergence,

$$\rho_M = -\nabla \cdot \boldsymbol{M}_S \tag{2}$$

If we assume that the thickness of the SCM is infinitely small, the magnetic scalar potential has a discontituity of magnitude as the dipole moment per unit area $|\rho_M h_S = f_s(x,z)$ at the double layer (ref.5). Then the governing equations for the potential are written as

$$\nabla^2 \phi_m = 0 \qquad (y \neq d_s) \tag{3.a}$$

$$\begin{cases} \phi_m^o(x,y,z) - \phi_m^i(x,y,z) = f_s(x,z) & (y = d_s) \\ \phi_m^o(x,y,z) + \phi_m^i(x,y,z) = 0 & (y = d_s) \end{cases} \tag{3.b}$$

where

$$\phi_m = \begin{cases} \phi_m^o & (y \geq d_s) \\ \phi_m^i & (y \leq d_s) \end{cases}$$

$$\boldsymbol{H}_S = (H_{Sx}, H_{Sy}, H_{Sz}) = -\nabla \phi_m$$

We then obtain the scalar magnetic potential as

$$\phi_m^{o,i} = \sum_{k=1,3,\cdots} \sum_{m=1,3,\cdots} \pm \frac{a_s(k,m)}{2} \sin \alpha_k x \cos \alpha_m z \cdot e^{\mp \beta_{km}(y-d_s)} \tag{4}$$

where

$\alpha_k = \pi k / L$, $\alpha_m = \pi m / H$, $\beta_{km} = \sqrt{\alpha_k^2 + \alpha_m^2}$

$$a_S(k,m) = \frac{32 n_s I_s}{\pi^2 k m} \sin(\alpha_k \frac{l_s}{2}) \sin(\alpha_m \frac{w_s}{2}) \frac{\cos(3\alpha_k \tau / 2)}{\cos(\alpha_k \tau / 2)} \cdot \sin(5\alpha_k \tau / 2)$$

$n_S I_S$: *mmf* of SCM, l_S , w_S : length and width of SCM, τ : pole pitch .

The flux linkages of armature windings for the three phases, the length of which corresponds to one section, are given by

$$\psi_U = \sum_{l=1}^{N_a/2} \left\{ \int_{x_{al}-\frac{3\tau}{2}+\frac{l_a}{2}-\lambda}^{x_{al}-\frac{3\tau}{2}-\frac{l_a}{2}-\lambda} \int_{-\frac{w_a}{2}}^{\frac{w_a}{2}} \mu_0 n_a H_{sy}(x', d_a - \frac{c_a}{2}, z') dx' dz' + \int_{x_{al}-\frac{\tau}{2}+\frac{l_a}{2}-\lambda}^{x_{al}-\frac{\tau}{2}-\frac{l_a}{2}-\lambda} \int_{-\frac{w_a}{2}}^{\frac{w_a}{2}} \mu_0 n_a H_{sy}(x', d_a + \frac{c_a}{2}, z') dx' dz' \right\}$$

$$\psi_V = \sum_{l=1}^{N_a/2} \left\{ \int_{x_{al}+\frac{7\tau}{6}+\frac{l_a}{2}-\lambda}^{x_{al}+\frac{7\tau}{6}-\frac{l_a}{2}-\lambda} \int_{-\frac{w_a}{2}}^{\frac{w_a}{2}} \mu_0 n_a H_{sy}(x', d_a - \frac{c_a}{2}, z') dx' dz' + \int_{x_{al}-\frac{5\tau}{6}+\frac{l_a}{2}-\lambda}^{x_{al}-\frac{5\tau}{6}-\frac{l_a}{2}-\lambda} \int_{-\frac{w_a}{2}}^{\frac{w_a}{2}} \mu_0 n_a H_{sy}(x', d_a + \frac{c_a}{2}, z') dx' dz' \right\}$$

$$\psi_W = \sum_{l=1}^{N_a/2} \left\{ \int_{x_{al}-\frac{\tau}{6}+\frac{l_a}{2}-\lambda}^{x_{al}-\frac{\tau}{6}-\frac{l_a}{2}-\lambda} \int_{-\frac{w_a}{2}}^{\frac{w_a}{2}} \mu_0 n_a H_{sy}(x', d_a - \frac{c_a}{2}, z') dx' dz' + \int_{x_{al}-\frac{11\tau}{6}+\frac{l_a}{2}-\lambda}^{x_{al}-\frac{11\tau}{6}-\frac{l_a}{2}-\lambda} \int_{-\frac{w_a}{2}}^{\frac{w_a}{2}} \mu_0 n_a H_{sy}(x', d_a + \frac{c_a}{2}, z') dx' dz' \right\} \tag{5}$$

where N_a is the number of cells, which is defined as one cell for two pole-pitch length, l_a, w_a : length and width of armature coil, c_a : distance between two layers, d_a : lateral position of armature coil, n_a : number of turn of armature coil, $x_{al} = (2 - N_a)\tau + 4(l-1)\tau$, $\lambda = 0$ (240-degree type), $\lambda = \tau / 6$ (120-

degree type), and the section is located at $-N_a\tau \le x' \le N_a\tau$.

The induced counter emf of armature coil is obtained by the equation

$$E_\zeta = \frac{d\psi_\zeta}{dt} \quad (\zeta = \mathrm{U, V, W}) \tag{6}$$

Now, we aim here to view the electrical variables from the $dq0$-axes, where the zero-sequence component appears due to the existence of the neutral line, i.e., $i_U + i_V + i_W \neq 0$. A transformation matrix that maps from three-phase axis to $dq0$-axeswith the power held constant is written as

$$C = \sqrt{\frac{2}{3}} \begin{pmatrix} \cos\theta_{dq} & \cos(\theta_{dq} - \frac{2\pi}{3}) & \cos(\theta_{dq} + \frac{2\pi}{3}) \\ -\sin\theta_{dq} & -\sin(\theta_{dq} - \frac{2\pi}{3}) & -\sin(\theta_{dq} + \frac{2\pi}{3}) \\ \frac{1}{\sqrt{2}} & \frac{1}{\sqrt{2}} & \frac{1}{\sqrt{2}} \end{pmatrix} \tag{7}$$

where $\theta_{dq} = \frac{x_1 + \lambda}{\tau}\pi$, $x_1(t) = x' - x = \int_{t_s}^{t} v_x(u)du$, $v_x(t)$: vehicle speed

In three-phase axes, the vector voltage equation becomes

$$\begin{pmatrix} V_U \\ V_V \\ V_W \end{pmatrix} = \begin{pmatrix} R & 0 & 0 \\ 0 & R & 0 \\ 0 & 0 & R \end{pmatrix} \begin{pmatrix} i_U \\ i_V \\ i_W \end{pmatrix} + \begin{pmatrix} L & M & M \\ M & L & M \\ M & M & L \end{pmatrix} \frac{d}{dt} \begin{pmatrix} i_U \\ i_V \\ i_W \end{pmatrix} + \begin{pmatrix} E_U \\ E_V \\ E_W \end{pmatrix} \tag{8}$$

Transformation of (7) by the mapping of (6) yields

$$\begin{pmatrix} V_d \\ V_q \\ V_0 \end{pmatrix} = \begin{pmatrix} R + pl_m & -\omega_{dq} l_m & 0 \\ \omega_{dq} l_m & R + pl_m & 0 \\ 0 & 0 & R + p(L + 2M) \end{pmatrix} \begin{pmatrix} i_d \\ i_q \\ i_0 \end{pmatrix} + \begin{pmatrix} E_d \\ E_q \\ E_0 \end{pmatrix} \tag{9}$$

where $V_d, V_q V_0$: source voltages, i_d, i_q, i_0: armature currents, $\omega_{dq} = d\theta_{dq}/dt$, R, L, M : resistance, self inductance, and mutual inductance between phases of armature, $l_m = L - M$. $p = d/dt$.

The interaction between the induced speed emf and the armature currents causes power dissipation, and accordingly leads to energy conversion from electric power to dynamic power via magnetic field. Finally, we get the propulsion force.

$$F_p = (E_U i_U + E_V i_V + E_W i_W)/v_x = (E_d i_d + E_q i_q + E_0 i_0)/v_x \tag{10}$$

otherwise, using the magnetic energy concept,

$$F_p = i^T{}_{dq0} C \left(\frac{dC^T}{dx_1} \psi_{dq0} + C^T \frac{d\psi_{dq0}}{dx_1} \right) \tag{11}$$

where $i_{dq0} = (i_d, i_q, i_0)^T$, $\psi_{dq0} = (\psi_d, \psi_q, \psi_0)^T$

Assuming sufficient control to keep the d-axis and zero-sequence currents at zero, the thrust coefficient K_F is defined as

$$K_F = F_p / i_q \tag{12}$$

And we have

$$K_F = -\sqrt{\frac{2}{3}}\sum_k\sum_m \alpha_k \Psi_{km}\left\{\sin\theta_{dq}\cdot g_{Ukm} + \sin(\theta_{dq}-\frac{2\pi}{3})\cdot g_{Vkm} + \sin(\theta_{dq}+\frac{2\pi}{3})\cdot g_{Wkm}\right\} \tag{13}$$

where

$$g_{Ukm} = e^{\beta_{km}c_a/2}\cos\alpha_k\left(x_1+\frac{3\tau}{2}+\lambda\right) + e^{-\beta_{km}c_a/2}\cos\alpha_k\left(x_1-\frac{\tau}{2}+\lambda\right)$$

$$g_{Vkm} = e^{\beta_{km}c_a/2}\cos\alpha_k\left(x_1-\frac{7\tau}{6}+\lambda\right) + e^{-\beta_{km}c_a/2}\cos\alpha_k\left(x_1+\frac{5\tau}{6}+\lambda\right)$$

$$g_{Wkm} = e^{\beta_{km}c_a/2}\cos\alpha_k\left(x_1+\frac{\tau}{6}+\lambda\right) + e^{-\beta_{km}c_a/2}\cos\alpha_k\left(x_1-\frac{11\tau}{6}+\lambda\right)$$

We also consider the model shown in Figure 2, which has 4-pole concentrated arrangement with 12-pole pitch space. The equations are slightly different from the case of the model-1, because the inner and outer armature coils have different number of turns, while they have the same value in the model-1.

Let's consider a feeding system such that the power is fed to the sections where the vehicle exists from three inverters to minimize the associated losses as shown in Figure 3. The block diagram is constructed based on the voltage equation (9), combining with the feeding system and the controller. We design a PI controller with cascade system, in which every inverter has its own current controller, for the speed control to demonstrate the performance. Moreover, disturbance compensations are added to the system, estimators of the speed emf and for the non-diagonal terms of the coefficient matrix that appears in (9). The variables with the symbol tilde indicate the estimated signals in the block diagram. The signals v'_0, v'_d and v'_q are the outputs of current controllers, whereas v_0, v_d and v_q are the compensated manipulated variables to be output from the inverters. The vehicle mass is denoted by

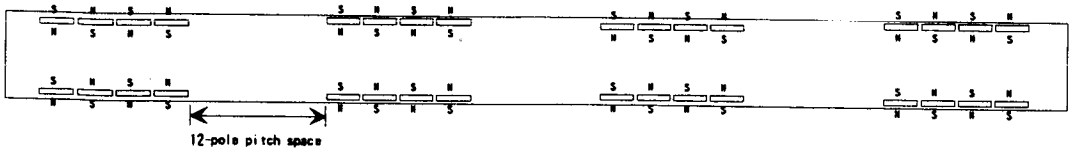

Figure 2. SCM arrangement of Model 2

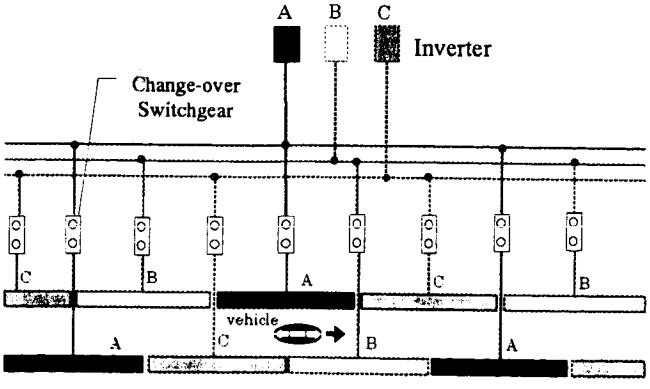

Figure 3. Three-power converter System

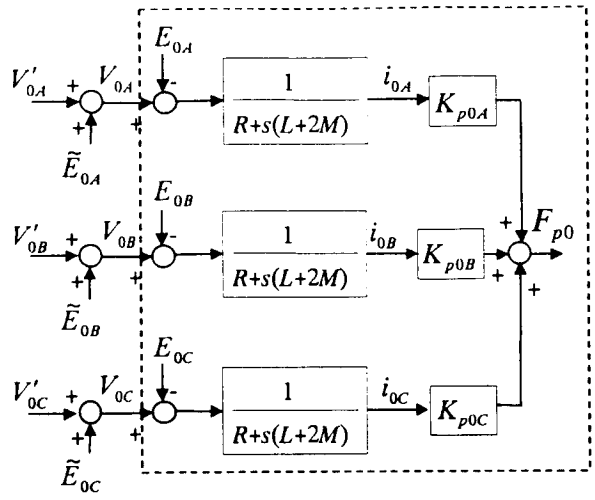

(a) Zero sequence

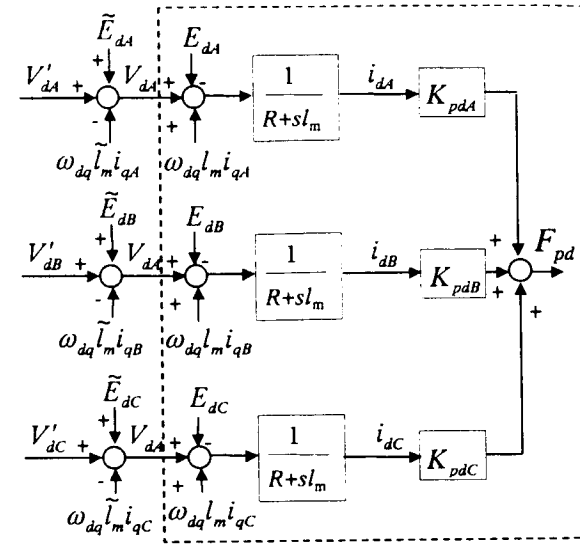

(b) d-axis

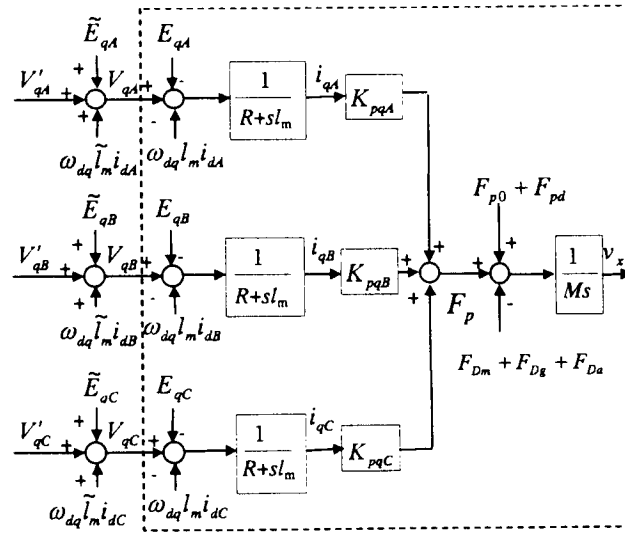

(c) q-axis

Figure 4. Block diagram of the control system

M. The forces F_{Dm}, F_{Dg} and F_{Da} are the drag forces resulting from the loss in magnetic levitation system, guideway gradient and air resistance that is proportional to the square of speed, respectively.

CALCULATED RESULTS

Figure 5 shows the speed emf induced in each one of the three-phase armature coils at the speed of 420km/h, which were calculated for the two cases of the 120-degree coil pitch type and the 240-degree coil pitch type. The comparison indicates that more high frequency components of emf are induced in the case of the 120-degree coil pitch type. As is easily seen, the amplitude increases and decreases when the vehicle enters and leaves the corresponding section, respectively. The thrust coefficients

calculated from (13) are shown in Figure 6. The values are shown for the single section case and the resultant case made up from neighboring sections. The resultant value is kept at some range near the steady value in either case, though the thrust coefficient changes between 0 to the resultant value for the single section. However, one noticeable thing is the severe pulsation for the 120-degree coil pitch type, resulting in possible high frequency dynamic force generation at SCM's even if the armature current itself is well controlled. In that respect, the 240-degree coil pitch type has better characteristics, but it still has a pulsation. It can be concluded that this pulsation appears due to the vehicle design where the number of the concentrated arrangement SCM is an odd number. This design brings about changing of the amplitude of the flux linkage with time for one section coil.

Accordingly, the vehicle should have even number of concentrated SCMs and Figure 7 shows the numerical example calculated for 2-pole concentrated arrangement of SCMs to prove this statement. In this case, the flux linkage amplitude is kept constant while the whole vehicle SCM's are positioned in one section as shown in Figure 7(a). Then the thrust coefficient has a constant value.

Next, we show the speed control simulations using the Model 2 with the three-power converter system. Two significant conditions are assumed: (i) The guideway has a tunnel. (ii) One of the 3 inverters, the inverter C, is disabled, and the corresponding circuit is opened so that unnecessary currents can't flow. Figure 8 shows the results. From the aerodynamic drag force profile, it may be understood that the speed control is working well as a result, because its value solely depends upon the vehicle speed other than the constants of the tunnel. On the normal guideway, the aerodynamic drag is about 50kN, and inside the tunnel it is about 90kN. Although the generated propulsion force follows well the aerodynamic drag except for some area, there appears rippled propulsion force at regular intervals. As mentioned earlier, the thrust coefficient has some steady value that is made from neighboring sections. But, these areas are where the vehicle runs partly on the section C, which is connected to the disabled inverter. Therefore, the thrust coefficient has ripples, producing the rippled forces. Propulsion force is controlled directly by q-axis current. Figure 8(c) shows the applied voltage of q-axis component at each section, where the C-section voltage is 0 from the assumption. During the period that the vehicle runs in the tunnel, the voltage amplitudes have larger values, and their profiles are almost proportional to the aerodynamic drag force. In Figure 8(d), the $dq0$ components of the inverter A are shown. The d-axis voltage has comparatively large value because it needs to cancel the coupling voltage from q-axis. The q-axis current value changes just as required to produce the propulsion force, while d-axis and zero-sequence currents are suppressed at almost zero as can be seen from Figure 8(e). Finally, the vehicle acceleration in the running direction is shown in Figure 8(f). The magnitude is small enough in spite of the rippled propulsion forces at some areas, which coincide with the time that the acceleration occurs. Our speed control system works well under the assumed conditions.

CONCLUSIONS

We have shown a methodology for the mathematical treatment of the superconducting linear synchronous motor, which makes it possible to define the thrust coefficient and to construct the speed control system block diagram. The formulation has been made in $dq0$-axis taking account of the space harmonic magnetic fields and time harmonic induced voltages of armature coils. First, it was found out that the vehicle-borne SCM should be arranged concentrically with even number of SCMs so as to not have rippled propulsion forces. Second, the speed control system was designed with the structure

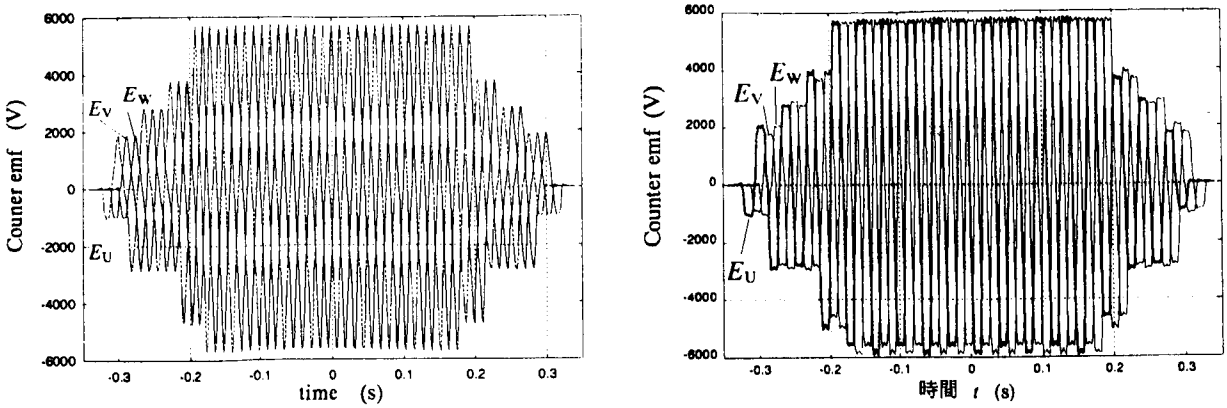

(a) 120-degree coil pitch with single layer

(b) 240-degree coil pitch with double layer

Figure 5. Counter emf for Model 1 (420km/h)

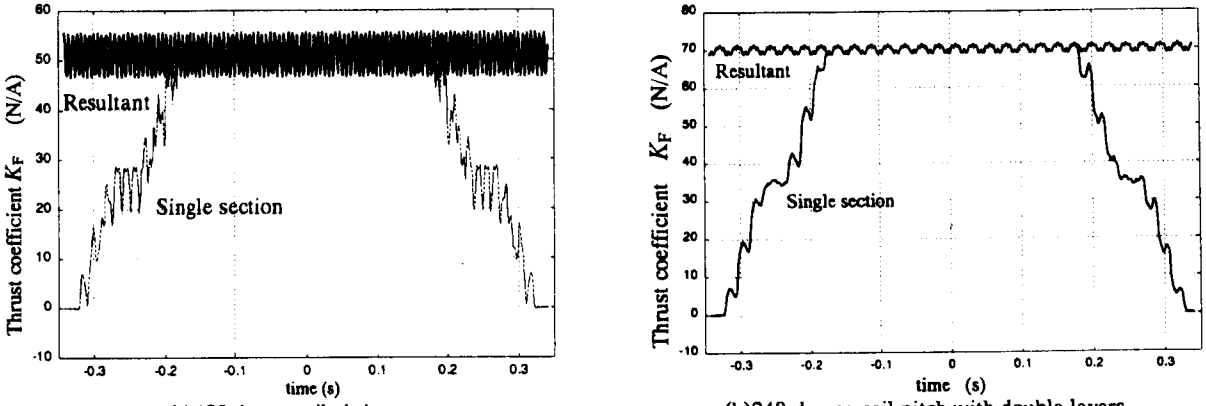

(a) 120-degree coil pitch type

(b)240-degree coil pitch with double layers

Figure 6. Thrust coefficient for Model 1 (420km/h)

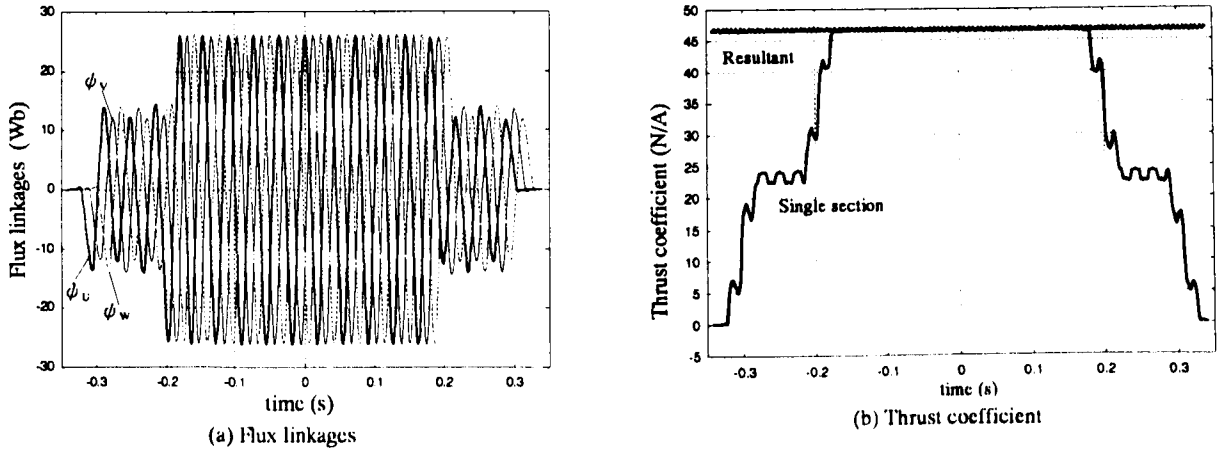

(a) Flux linkages

(b) Thrust coefficient

Figure 7. 2-pole concentrated arrangement of SCM with 4-pole space (420km/h)

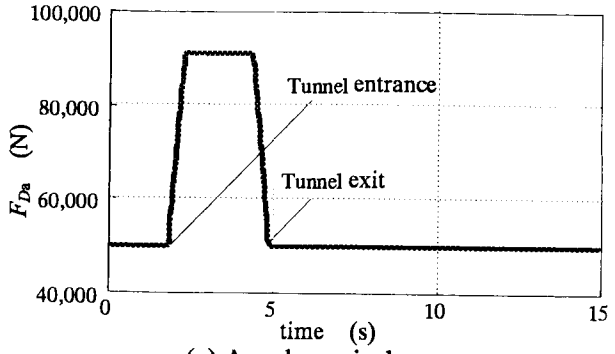

(a) Aerodynamic drag

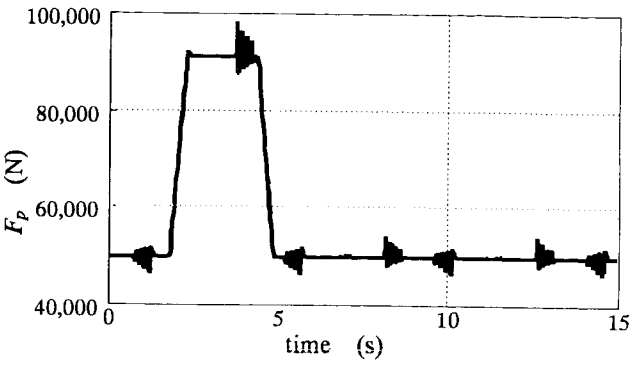

(b) Propulsion force

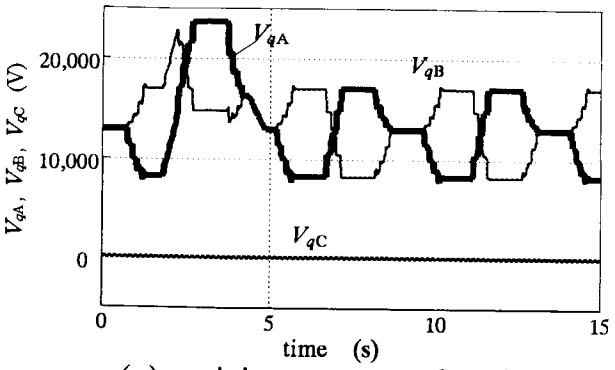

(c) q-axis inverter output voltage for A-, B- and C-section

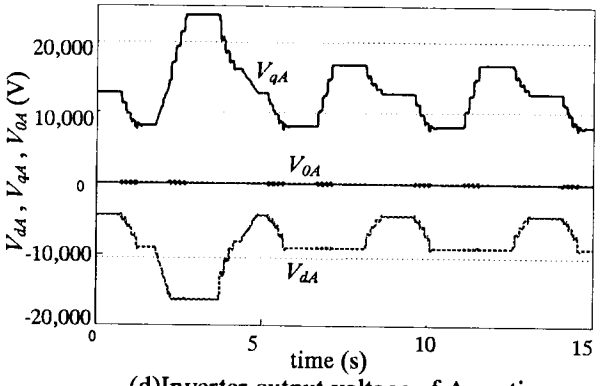

(d)Inverter output voltage of A-section

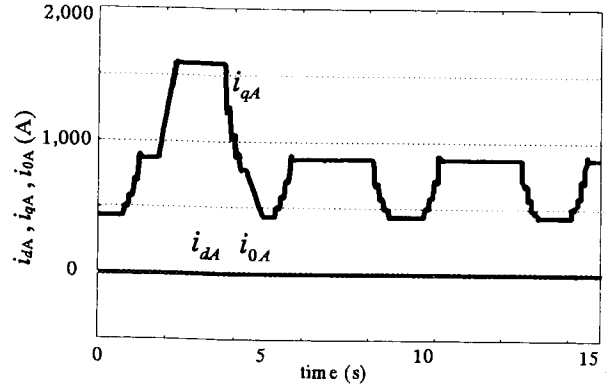

(e) Currents of A-section

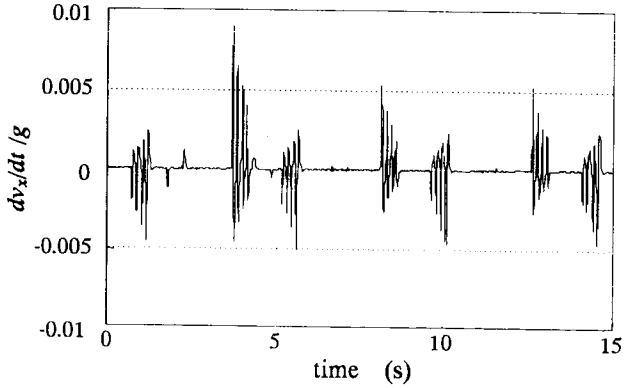

(f) Ratio of vehicle acceleration to gravitational acceleration

Figure 8. Speed control simulation with the disabled inverter C for Model 2 (Speed reference: 550km/h)

of the power feeding system comprised of three inverters. Computer simulations have shown that the speed control system works well under the condition that the guideway has a tunnel and one of the inverters is disabled.

REFERENCES

1. G.E.Dawson, P.C.Sen, D.J.Clarke and S.Lakhavani, Linear Synchronous Motor Feedback Controls, *IEEE Trans. Magn.*, vol.12, pp.885-888, November 1976

2. N.Maki, H.Okuda, J.Fujie and T.Iwahana: A Combined System of Propulsion and Guidance by Linear Synchronous Motors, *IEEE Trans. Power Apparatus and Systems*, vol.96, No.4, pp.1109-1116, 1977

3. H.Ikeda and I.Kawaguchi, Development of Thrust Control System for Linear Synchronous Motor, *Trans. IEE of Japan*, vol.108-D, No.8, pp.757-764 , 1988

4. T. Sakamoto, Analysis of a Superconducting Linear Synchronous Motor Propulsion in Terms of *dq* Variables, *Trans. IEE of Japan,* vol.116-D, No.2, pp.177-182, 1996.

5. W. Panofsky and M. Phillips: Classical Electricity and Magnetism. Addison-Wesley Publ. Co., 1977.